Mini Cheetah ‘Pro’: Design, Analysis, + Fabrication of a Highly Dynamic Quadruped Robot

Aditya Mehrotra
Biomimetic Robotics Lab
PI: Professor Sangbae Kim (PhD), SV: Elijah B. Stanger-Jones (SM)
Massachusetts Institute of Technology
Email: adim@mit.edu

Abstract. *Mini Cheetah was designed to be a robust quadruped robot capable of highly dynamic motions enabling controls engineers to test more aggressive and optimistic algorithms on hardware—while still being small enough to be safely operated by one researcher. Since the Mini Cheetah was designed, actuation modules with higher power density and more robust electronics have been designed, and more powerful and efficient computers have been developed. Mini Cheetah 'Pro' is a redesigned version of the Mini Cheetah with (4x) the power density and (1.15x) larger limbs. It also has improved structure, ease of assembly, and overall serviceability. Here we present the design of Mini Cheetah 'Pro' as specific and strategic upgrades to the original Mini Cheetah. We also present design verification in the form of dynamometer motor testing and simplified simulation results to show the new platform will have increased dynamic capabilities over the old one. We end with a discussion on future work necessary for the project.*

I. Introduction

The Mini Cheetah platform—as designed by Ben Katz—is actively used in most of the quadruped controls research that happens in the Biomimetic Robotic Lab [1]. When designed, the platform pushed the capabilities of dynamic legged robots far with its high power to weight ratio, inexpensive actuation paradigm, and impact-robust mechanical design. But over the years since it was first designed, the Mini Cheetahs of MIT have been through a lot. Because of continued testing researchers are seeing more frequent hardware failures which is requiring more and more time spent on maintenance.

Technology has also improved. The lab has designed actuators with over (4x) the peak power density in similar package sizes to the original actuators, and a higher performance power and communications system [4][9]. UpBoard and Nvidia now have new computers with multiple times the processing power that the Mini Cheetah did in a similar form factor [2][3]. And as the labs other robots transition to the newer electronics platform and newer compute systems, two main issues arise [4]. First, comes a significant reduction in ability to maintain the Mini Cheetah platforms as the lab simply no longer has the parts to fix the robot (the new robots use significantly different parts) [4]. Second, comes the fact that controls research is increasingly limited by the lack of compute power on-board the robot itself [16]. A re-design to increase our ability to maintain the platform while also increasing overall platform performance, is certainly worth the significant effort it takes.

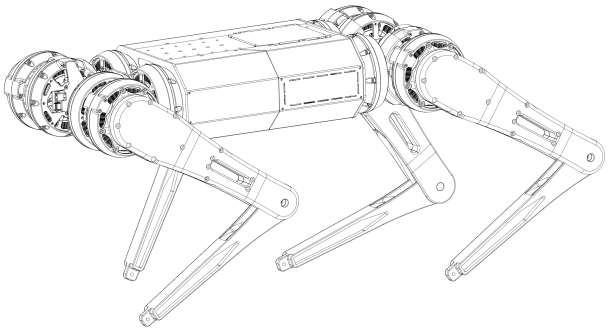

Fig 1. The new Mini Cheetah ‘Pro’ design isometric view in CAD sketch.

Another motivation for re-design is re-design, especially when starting from an already well designed system, leaves room to properly document design process as well as the system itself. Good documentation can increase the service life of a robot far into the future, and it provides a learning resource for others to build off our work.

I.1.0 Method + Results. We will take the approach of comparing our new design to the design of the original Mini Cheetah as presented in [1]. This will involve side-by-side comparisons of the mechanical design, actuation, transmission, and electrical systems. We will additionally present a design verification in the later sections of the paper which includes the development of a dynamometer motor testing platform for direct torque speed comparisons between actuators, and the use of trajectory optimization simulation in MATLAB to provide initial comparisons between the dynamic performance of the new and old robot. For additional motivations for legged robots and controls research for legged systems, see [1] and [5].

II. Design

The Mini Cheetah Pro's design builds on the work of the Cheetah 3 [5] and the Mini Cheetah [1] platforms providing a more power dense and robust, robotics system for controls research. Systematic upgrades were performed on the platform in the areas of electrical design, mechanical design,

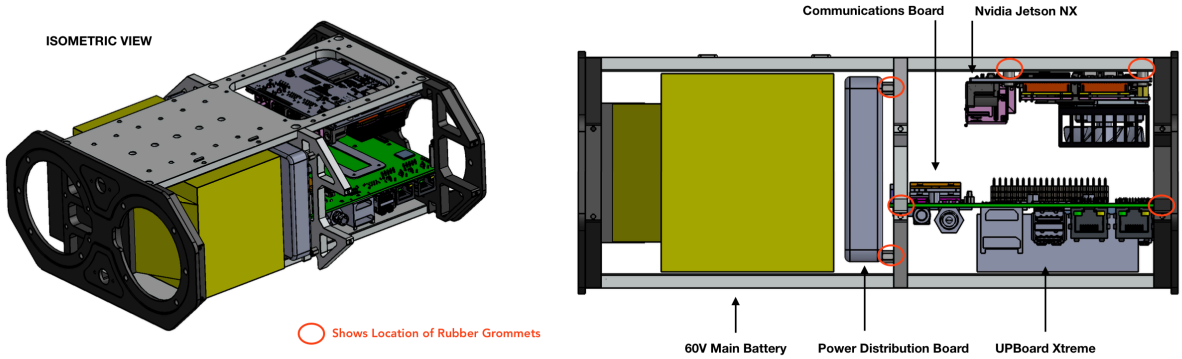

Fig 2. (left) 3D view of the core in CAD, (right) side view of the core in CAD with the battery, power distribution board, computers, and communications board labeled. Red circles show the location of rubber grommets for PCB protection.

actuation, communications, and user-centered design. The new platform is shown in Fig 1. The platform's body size is roughly (1.06x) bigger than the original platform and the link lengths are around (1.15x) larger. The body scale-up represents the minimal scale-up required to fit the new electronics system, the leg scale-up was chosen to give the robot a slightly higher ground clearance for avoiding obstacles. A summary of the robot's specifications is shown in Table 1.

Table 1. Mini Cheetah Pro Specifications

Whole Robot Properties	
Mass (est.)	11-14 (kg)
Overall Length	0.314 (m)
Body Width	0.200 (m)
Body Height	0.105 (m)
Leg Properties	
Link Length	0.240 (m)
Belt Reduction (knee)	28t:18t

**(est.) stands for estimated from CAD, real measurements will be taken on assembly.*

II.1.0 Design of the Central Core. The new robot has a stronger and more robust mechanical design than its predecessor and added space for more advanced electronics —much of this has to do with the design of its new structural core.

The central core consists of three main ribs, a top plate and a bottom plate. The entire core is made of CNC'ed 6061-T6 Aluminum (anodization level III) as opposed to the 3D printed plastic ribs of the Mini Cheetah. All ribs double as mounting structures. As see in Fig 2, the left-most rib serves as mounting for the battery, and the front two abduction-adduction (ab-ad) motors. The middle rib provides support for the main power distribution board, the RC receiver, the IMU, and one of the two computers/communications board. The right-most rib supports the other half of the computer stack as well as the rear two ab-ad motors. Because the core is structural and will take loads from the robot's legs and the environment, electronics are mounted to the core with rubber grommets in between the PBCs and the structure itself. This allows the core to flex and absorb impact without requiring the PCBs to flex as well (PCB flex is undesirable and could lead to failure).

The top plate has mounting holes for both the secondary computer system as well as any accessories we wish to mount to the top of the robot. The bottom plate is simply a supporting plate with no specialized mounting holes. All of the ribs, and the top and bottom plate have mounting holes to attach to each other as well as the side body panels. All components have pockets that strategically minimize the mass of the core while still maintaining a strong structure. This rib-based design allows for minimization of overall body size.

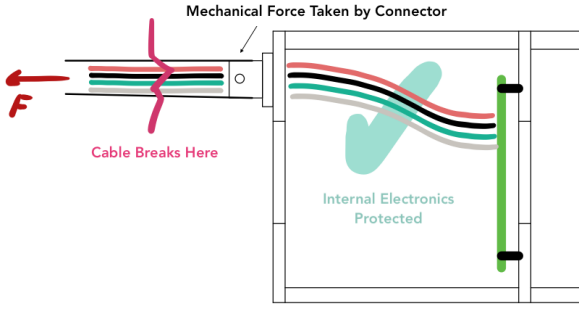

Fig 3. Connectors such as the AS-07 race-spec series take forces applied to the cable harness. If the motor cables external to the body get caught on obstacles or the legs themselves only exterior portions of the cable will be damaged, internal connections and PCBs will remain un-harmed.

II.1.1 Electrical Connectors. The new core and body design also incorporate the use of specialized electrical connectors which provide mechanical locking in addition to electrical pin connections. The previous design simply ran the power and data cables to exterior motors through a hole in the body so if the cable saw strain forces components internal to the body of the robot could be damaged as well. The new design uses AS-07 race-spec connectors which prevent any forces on the external cable harness from being transmitted to the cabling or PCBs housed inside the body. This makes repairs easier in the event of damage as damaged cabling is easily accessible without opening the main body of the robot [4]. This is shown in Fig 3.

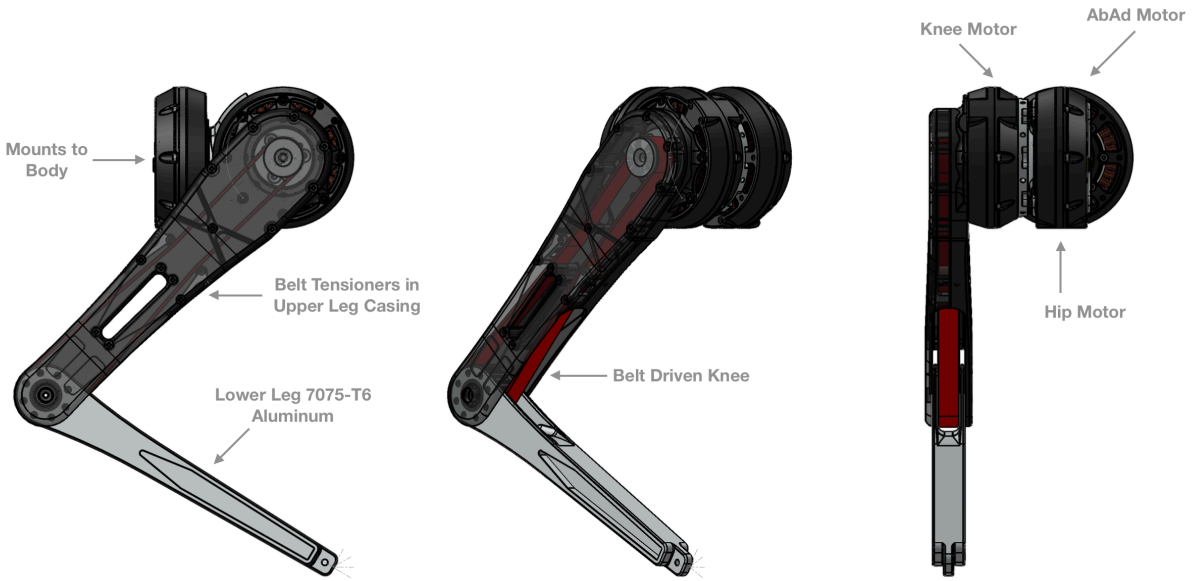

Fig 4. View of the leg design in CAD with the hip, knee, and ab-ad motors labeled. A belt is used to drive the actual knee joint which allows for an additional 28t:18t gear reduction at the knee (the same as the original Mini Cheetah). This design also minimizes the inertia of the legs which helps with mitigating impact forces.

II.2.0 Leg Design. The leg design of the new robot is very similar to that of the old robot. There are only two major changes—the design of the mechanical mount between the hip and knee motors, and the actual choice of belt used to drive the knee. The general design of the leg and labels of ab-ad, hip, and knee motors are shown in Fig 4. More detailed explanation of the general leg design can be found in [1].

II.2.1 Hip/Knee Motor Interface. A diagram associated with this section is presented in Appendix A.1.0. The knee motor on the Mini Cheetah generally takes the most abuse as it is the most exposed and absorbs most of the impacts with the environment. This results in frequent replacement of that motor. The hip/knee motor interface was redesigned purely for purposes of assembly. The previous design utilized screws that were driven perpendicularly into the back face of the knee motor. Because of the minimal clearance between the back face of the knee motor and the front face of the hip motor (~16.5mm), specialized tooling was required to assemble and disassemble this system which resulted in an annoying and time consuming process. The new design requires more parts but uses screws driven radially which enables the use of traditional tooling for assembly and disassembly of the system. The process is also faster as alignment of the screws is easier [7]. In the future we may quantify the time to replace the knee motor on the new platform compared to the old, but for now we rely on the general design for assembly principals presented in [7]. When designing this new structure, torque transfer at the hip was considered as well as the entirety of the hip motor torque capabilities are transferred to the leg through this assembly.

II.2.2 Belt Design Considerations. As shown in [1] and [8], leg designs involving a belt can decrease leg inertia and increase impact mitigation capabilities but also suffer from limited torque control bandwidth. Torque control bandwidth refers to the maximum frequency of the torque command going to the motor a system can achieve, which also tells us how "reactive" the robot can be to certain situations [5]. The limitation comes from the fact that a belt is not infinitely stiff, it has a "springiness" related to it. The knee motor is trying to drive the knee link but in between the two there is a stiff spring. This means there is a mechanical resonance between the motor rotor and the belt itself which limits the frequency of the command we can send before the system starts to resonate. In the original Mini Cheetah this number was 30Hz [1][8]. We want the belt resonant frequency to be equal to or higher than this value for the new platform.

The frequency of the resonance depends on the belt stiffness and the inertia of the motor. Table 2 shows the new motor modules (U10) have roughly double the inertia of the old modules (U8). This means the belt stiffness will have to increase to mitigate the increase in inertia based on the general form for mechanical resonance $f = \sqrt{(k/m)}$.

Table 2. U10 vs. U8 Actuator Specifications from [4] and [8]

U10 Actuator @ 60V	
Mass (est.)	0.619 (kg)
Stall Torque	33 (Nm)
Free Speed	35 (rads/s)
Rotor Inertia (est.)	0.0040 (Kgm^2)
Gear Reduction	6:1
U8 Actuator @ 24V	
Mass (est.)	0.480 (kg)
Stall Torque	17 (Nm)
Free Speed	40 (rads/s)
Rotor Inertia	0.0023 (Kgm^2)
Gear Reduction	6:1

**(est.) stands for estimated from CAD, real measurements will be taken on assembly.*

Belt stiffness is proportional to the free-span length (the unsupported length between the pulleys), the width, and the material. The effects of these properties on stiffness are summarized in Appendix A.2.0 and a simplified model of the leg is shown in Appendix A.2.1. The leg length increasing by (1.15x) means an increase in free-span length by the same factor. Based on this the design decision was made to switch

from a Kevlar to a Carbon Fiber belt and increase the width of the belt from 9mm to 15mm. The calculation is shown below. K is belt stiffness, J is rotor inertia, "old" and "new" refer to the original platform as compared to the new one.

Scale the stiffness and inertia.

$$K_{new} = K_{old} * 2.0 * 1.5/1.15 = 2.61 * K_{old}$$

$$J_{new} = J_{old} * 2.0$$

The belt is (1.5x) wider, so stiffness increases by (1.5x).

Carbon belts are (2x) as stiff as Aramid belts.

Use the basic mechanical resonance formula.

$$f_{new} = \sqrt{(K_{new}/J_{new})} = \sqrt{(2.61 * K_{old}/J_{old} * 2.0)}$$

$$= f_{old} * 1.14 \quad = 34$$

The torque control bandwidth of the new platform can be estimated to be around 34Hz. This is a (1.13x) safety factor over the minimum bandwidth. The safety factor is important in this case because this calculation does not include considerations such as tooth deflection and other modeling errors which can decrease the actual stiffness of the belt [8]. When the platform is assembled we will measure the actual resonant frequency to determine bandwidth.

II.3.0 Actuation + Electrical System Design. As shown previously in Table 2 and described earlier, the new platform uses upgraded actuators. The higher performance comes from a combination of using a more powerful motor core and upgraded motor driver, as well as increasing the system voltage to 60V. The design of the actuator is presented in [9], and the new electrical system design is presented in [4]. Verification, testing, and power density calculations for the new actuation system are presented in Section III of this paper.

III. Verification

We used a combination of both hardware testing and MATLAB simulation to provide some initial comparisons between the performance of the two platforms. Hardware testing took the form of dynamometer motor testing of the U10 motor modules to compare to data collected in [8]. The simplified MATLAB simulation provides a comparison between a 1-Degree-of-Freedom (1DoF) version of a single leg of Mini Cheetah and the same for Mini Cheetah 'Pro' performing the task of jumping. Readers are encouraged to read [10] before reading this section if they are unfamiliar with dynamometer motor testing. Motor torque speed curves and power maps can be found in Appendix B.1.

III.1.0 Dynamometer Motor Testing. A dynamometer is a device used to characterize the performance of a motor. It features a testing motor, a motor under test, a current sensor and voltage sensor at the input of the motor controller, and a mechanical torque sensor between the two motors. A picture of the test setup is shown in Fig 5 and a more detailed description of the setup is presented in [10] but a summary will be given below.

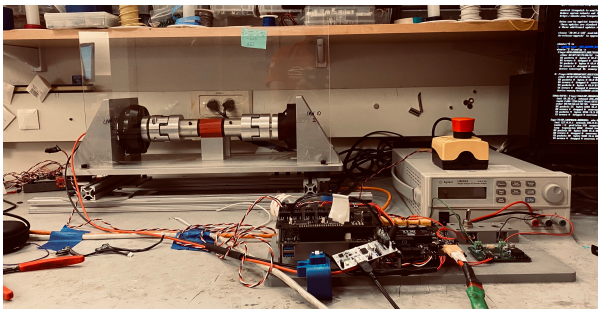

Fig 5. A picture of the motor testing setup including the two motors, the power supply, logging board, and sensor suite.

III.1.1 Description of the Dynamometer Platform. Dynamometers are used to measure the torque-speed curve of a motor system (the motor, motor controller, and gearbox together as a unit as all affect each other's performance capabilities). A motor's performance capabilities are defined by the maximum torque it can produce at a given speed where these limits are defined purely by physics, specifically electromagnetism [17]. To measure this curve, a motor of equal or higher power capabilities than the motor we are trying to test is placed under PID velocity control. This motor, called the testing motor, sets the speed of the system. The motor under test is the motor we are trying to measure the torque-speed curve of, we command the torque of this motor to be in the same direction as the velocity of the motor under test. We increase this torque command until the motor can no longer achieve the desired torque at the desired speed. We repeat this process for a series of velocities in the range of 0 rads/s to the free-speed of the motor. This coupled with stall tests, free-speed tests, and interpolation allows us to build up the torque speed curve of the motor [4][10].

Our dynamometer platform uses a FUTEK 100Nm analog torque sensor, the power board from the Mini Cheetah 'Pro' and MIT Humanoid platforms [4], and an UPBoard Xtreme running Ubuntu 18.04 and custom software. The computer is connected to the same CAN Transceiver board used in the Mini Cheetah 'Pro' and MIT Humanoid platforms [4]. The computer communicates with the transceiver board using SPI and the board communicates with peripherals using CAN. We designed a separate PCB that takes in signals from the FUTEK torque sensor and sends them over CAN to the transceiver board from which the signals can be read by the computer. The power board also reports voltage and current data over CAN to the transceiver board. The setup is shown in Fig 6 on the next page.

III.1.2 Optimizing the Communications Stack. Because a lot of a motor's transient behaviors occur very quickly—especially ones we are interested in—we determined the dynamometer itself should have data acquisition and logging rates no less than 2.5kHz. This speed was determined through experimentation to be fast enough to measure the motor's electrical dynamics [4]. This isn't strictly necessary for full module characterization but is very helpful when tuning the motor controllers which is essential for accurate full-system characterization [4][8].

The main bottleneck for achieving the desired logging rate is the Serial Peripheral Interface (SPI) between the computer and the Transceiver Board (SPIne Board). This is because the

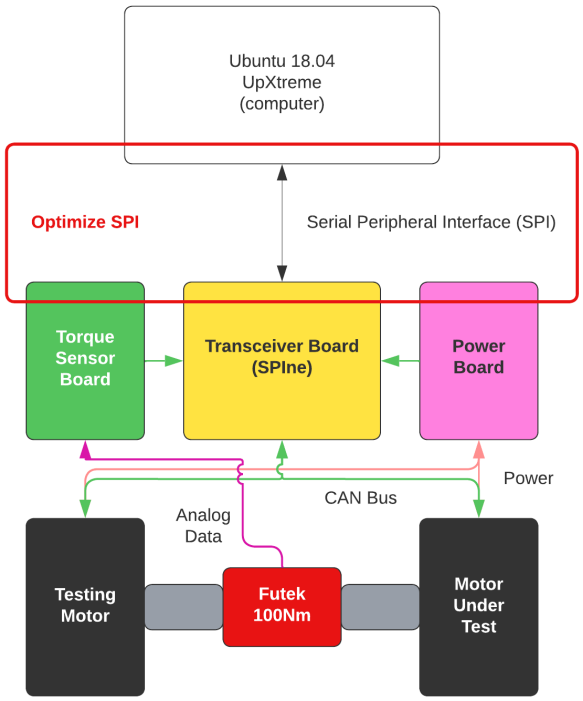

Fig 6. Communications architecture of the dynamometer platform. Our communications speed optimization focused on the SPI interface between the main computer and the transceiver board (SPIne board).

SPIne board has six CAN interfaces distributed across two STM32 microcontrollers meaning each CAN interface only needs to handle the data for a single motor or peripheral PCB in this system [4]. At each sampling interval, all the data from both motors, the torque sensor, the power board, and any other sensors must be read by the SPIne board and then transferred in a single data structure to the computer over SPI for logging. At the same time, the computer is sending back control data to the SPIne board to send to the motors. Due to the desired 2.5kHz logging rate, this needs to happen in less than a 400us sampling interval.

We first determined the minimum number of bytes required to fully represent the data that needed to be transferred between the SPIne board and computer. By defining a minimum and maximum value for each of the fields in the data structure, we determined 76 bytes would be needed for reliable communication between the two devices without overflow or corruption. This translates to 608 bits of data being transmitted between the two devices during each sampling interval. To do this in 400us, we need a data transfer rate of 1.5Mbps. By minimizing the size of the data structs and using a SPI data transfer speed of 2Mbps, we were able to achieve greater than the desired 2.5kHz sampling rate.

III.1.3 Motor Testing Results. Testing revealed that the U10 motors could produce a maximum of 33Nm at a speed of 28rad/s compared to the U8 motor 17Nm at 10rads/s. The U10 motor mass only increased to 620g from the U8 motor 480g. We can calculate the peak power P and the power density ρ (defined as the peak mechanical power over the mass of the actuator) as follows. We calculate these numbers for the full actuator module including the 6:1 gear ratio.

Mechanical power is torque times velocity.

$$P_{U8} = 16.5 * 10 \approx 165 \text{ W}$$

$$P_{U10} = 33 * 28 \approx 925 \text{ W}$$

For power density divide by actuator mass in Kg.

$$\rho_{U8} = P_{U8}/0.480 \approx 343 \text{ W/Kg}$$

$$\rho_{U10} = P_{U8}/0.619 \approx 1494 \text{ W/kg}$$

That's over (4x) the power density on the new motor modules.

Based on this, we can see the U10 has close to (4.36x) the power density of the U8 actuator. We estimate this increase in power density will offset the overall platform mass increase of (1.5x) and the link lengths increasing by (1.15x) to yield overall higher performance [11].

III.2.0 Verifying Intuition w/ Simulation. For those unfamiliar with trajectory optimization, we recommend Matthew Kelly's trajectory optimization tutorials linked in [13]. It is, however, important to note the details of the trajectory optimization are besides the main point. We encourage readers to skim the details but read section III.2.2 which presents the results of the simulation comparison between the new and old Mini Cheetah platforms.

To initially test the theory that the new platform will have overall better performance than the previous platform (in addition to being more reliable and robust), we ran a simple trajectory optimization simulation in MATLAB based off work done by Matt Chignoli and Charles Khazoom for [11] and work we did for a separate project [12]. We modeled just the leg of the new and old Mini Cheetah platforms in terms of lengths, masses, and inertias. We then constrained the foot and hip to only move along the vertical direction for all time. A single actuator (either a U10 or U8 depending on the platform) was placed at the hip and a maximum jump height optimization was formulated using the direct collocation strategy [13][14].

III.2.1 Optimization Formulation + Modeling. To ensure the accuracy of the simulation, we used a motor modeling strategy we presented in a separate project linked in [12] and summarized here. This consisted of three constraints on the actuator effort. First, the motor torque must be less than the max torque (or saturation torque) of the torque-speed curve. Second, the speed must be less than the max speed on the curve. Third, the torque and speed point must lie under the line that represents the max torque the motor can provide at a given velocity especially at the higher velocities (the downward sloping line on the torque-speed curve). The overall formulation of constraints is shown below.

The torque limits of the motor. Where U_i is the command at each time step.

$$-\tau_{max} <= U_i <= \tau_{max}$$

The speed limits of the motor. Where V_i is the velocity at each time step.

$$-\omega_{max} <= V_i <= \omega_{max}$$

Torque-speed curve constraint, usually not present in optimizations.

$$U_i <= m_t V_i + b_t$$

*Where the line y = mt * x + b represents the motor's performance limit line.*

Other standard constraints such as the ground may only exert upwards forces on the foot, the leg cannot penetrate the ground, and dynamics were all employed as well but not discussed in this paper. The simulation used simple Euler Integration between time-steps. The optimization code is linked in [15].

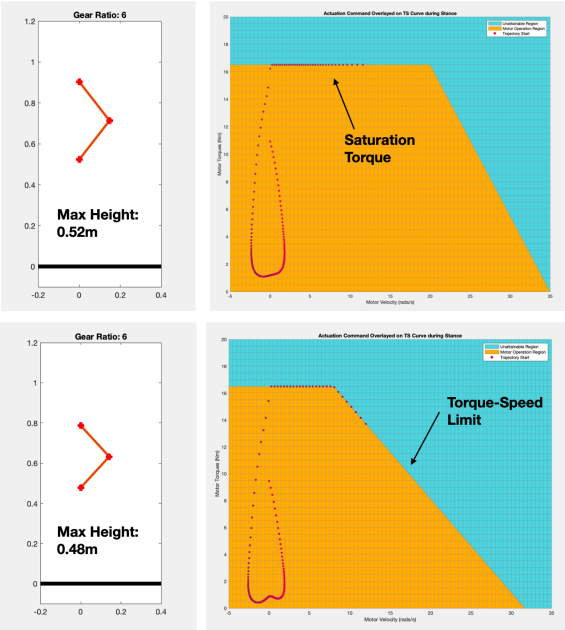

Fig 7. Results from simulation (top) Mini Cheetah 'Pro' (bottom) Mini Cheetah. The new leg jumps 4cm higher than the old one with this lower-order model.

III.2.2 Optimization Results. The main focus of this optimization was to determine—with a simplified model of the leg and actuator—if we could see a performance increase in the new platform as compared to the old one. Proper comparisons would have to happen on real hardware or using more detailed simulation in the future—but the initial results shown in Fig 7 are promising. The Mini Cheetah 'Pro' leg jumps around 4cm higher than the original Mini Cheetah leg and uses less of the actuator's full capabilities to do so. This 4cm difference is significant for the purposes of a 1DoF jumping leg [11][12].

It is important to note there are many inaccuracies in the optimization above. Both platforms have an actuator acting at the knee which this simulation does not have. Both platforms inertias, masses, link lengths, and other parameters are not modeled exactly in this simulation—they're simply "close enough" values from CAD. This means our simulation results cannot be conclusive, they are just an initial estimate of comparisons between the dynamic performance of the two robots.

IV. Discussion + Future Work

The project is far from complete, we are currently in the stages of manufacturing the platform and challenges such as the pandemic's impact on the global supply chain are slightly slowing progress. All mechanical parts have been sent out for manufacturing and the electronics needed have been ordered.

We estimate parts to arrive around mid-end June after which we will begin the process of assembly, testing, and verification. This process involves mechanical assembly of the robot, testing and bringup of the electrical components, and system characterizations. This includes measuring the real mass and inertias of the body and links as well as measurements of the actual rotor-belt resonant frequency to determine the platform's torque control bandwidth.

We estimate we will start to deploy controls algorithms onto hardware in late Fall. Before we do so, we would like to expand the 1DoF leg simulation in this paper to a more accurate 2DoF simulation with parameters measured during assembly of the physical robot. This will provide us with initial estimates of what full platform simulation results should look like and what comparative behaviors the new platform should be able to perform. In addition, calculations regarding the effective mass of the legs in the sagittal plane and the Impact-Mitigation-Factor (IMF) of the robot will all be beneficial to comparing the new platform to the Mini Cheetah and Cheetah 3 and for developing controls algorithms [5]. For any results deployed to real hardware, we will perform a sim-to-real comparison to better characterize any discrepancies we see on the real platform versus in modeling.

Future work with the new platform will also involve integrating a perception stack and perhaps more compute power for research in the areas of state estimation through impact and contact, as well as general robot navigation, foot placement, and obstacle avoidance. This will include designing better accessories for the robot including camera mounts, carry handles, roll cages to protect sensors and more. The foot itself still needs to be designed as well. We are currently experimenting with using FormLabs SLA printers and additive manufacturing to create new, more optimized foot designs.

We hope to show these results as well as examples of new and exciting dynamic behaviors the robot can perform in future white-papers, presentations, and videos.

V. Conclusion

This paper presented the design and preliminary analysis of the Mini Cheetah 'Pro' platform, an upgraded version of the Mini Cheetah designed and built by Ben Katz [1][8]. We performed systematic upgrades to the original design to increase the durability, service life, and performance of the robot. We showed the new actuators significantly out-perform the old actuators and initial simulation results are encouraging. Future work involves the assembly, bring-up, and real world testing of the robot, the results from which will finalize the new platform's comparative abilities to the old one. Overall, we are excited for the new Mini Cheetah platform and the possibility of the new and more 'awesome' controls work we can do with it.

VI. Acknowledgements

Acknowledgements are presented in long-form after the appendices. As this work turns the last page in my undergrad career, I had too many people I wanted to thank.

VII. References

[1] *J. D. C. Benjamin Katz and Sangbae Kim, "Mini Cheetah: A Platform for Pushing the Limits of Dynamic Quadruped Control," International Conference on Robotics + Autonomous Systems (ICRA), 2019*

[2] *F. Serzhenko, "Benchmark Comparison for Jetson Nano, TZ2, Xavier NX and AGX," Fast Video GPU Image Processing, N.D.* https://www.fastcompression.com/blog/jetson-benchmark-comparison.htm

[3] *N.A., "UP Board, Modules + Systems," Texim Europe, N.D.* https://www.texim-europe.com/serie.aspx?name=UP

[4] *E. B. Stanger-Jones, "Expanding the Capabilities of Dynamic Robotic Systems," Department of Electrical Engineering + Computer Science, Massachusetts Institute of Technology, 2022*

[5] *G. Bledt, M. J. Powell, B. Katz, J. Di Carlo, P. M. Wensing, and S. Kim, "MIT Cheetah 3: Design and Control of a Robust Dynamic Quadruped," 2018 IEEE/RSJ International Conference on Intelligent Robots and Systems (IROS), 2018.* doi: 10.1109/IROS.2018.8593885

[7] *G. Boothroyd, P. Dewhurst, W. A. Knight, "Product Design for Manual Assembly," CRC Press, 2010.*
ISBN: 9780429142963

[8] *B. Katz, "A Low Cost Modular Actuator for Dynamic Robots," Department of Mechanical Engineering, Massachusetts Institute of Technology, 2018.*

[9] *A. Hattori, "Design of a High Torque Density Modular Actuator for Dynamic Robots," Department of Mechanical Engineering, Massachusetts Institute of Technology, 2020.*

[10] *A. Mehrotra, "Dynos for Dummies (And other interesting motor things…)," Department of Alchemy, 2022.* https://www.adim.io/_files/ugd/067a81_c7165eb397794bbf8eab9d27706da229.pdf

[11] *Professor Sangbae Kim, MIT 2.74: Bio-Inspired Robotics, Fall 2021.*

[12] *F. Gillespie, A. Mehrotra, "Gear Ratio Optimization for a Jumping Mini Cheetah," MIT 6.832 Underactuated Robotics, Spring 2022.* https://github.com/fgillespie66/gear_ratio_optimization_matlab

[13] *M. Kelly, "Trajectory Optimization - Learning the Theory," Matthew Kelly, N.D.* http://www.matthewpeterkelly.com/tutorials/trajectoryOptimization/index.html

[14] *Professor Russ Tedrake, MIT 6.832: Underactuated Robotics, Spring 2022.*

[15] Optimization Code: https://github.com/adimehrotra/mc_pro_comparison

[16] *G. Bledt, "Regularized Predictive Control Framework for Robust Dynamic Locomotion," Department of Mechanical Engineering, Massachusetts Institute of Technology, 2020.*

[17] *S. H. Kim, "Electric Motor Control," Elsevier Science, 2017.*

[18] *T. Kis, Mathworks, Github.* https://github.com/tamaskis/line_intersection-MATLAB

[19] *J. Andersson, J. Gillis, G. Horn, J. B. Rawlings, and M. Diehl. "CasADi—A Software Framework for Nonlinear Optimization and Optimal Control," Mathematical Programming Computation, 2018.* https://web.casadi.org

Appendix A.

A.1.0 Assembly comparison between old and new mini cheetah hip/knee mounting. The old system is shown on the bottom, the new system is shown on the top.

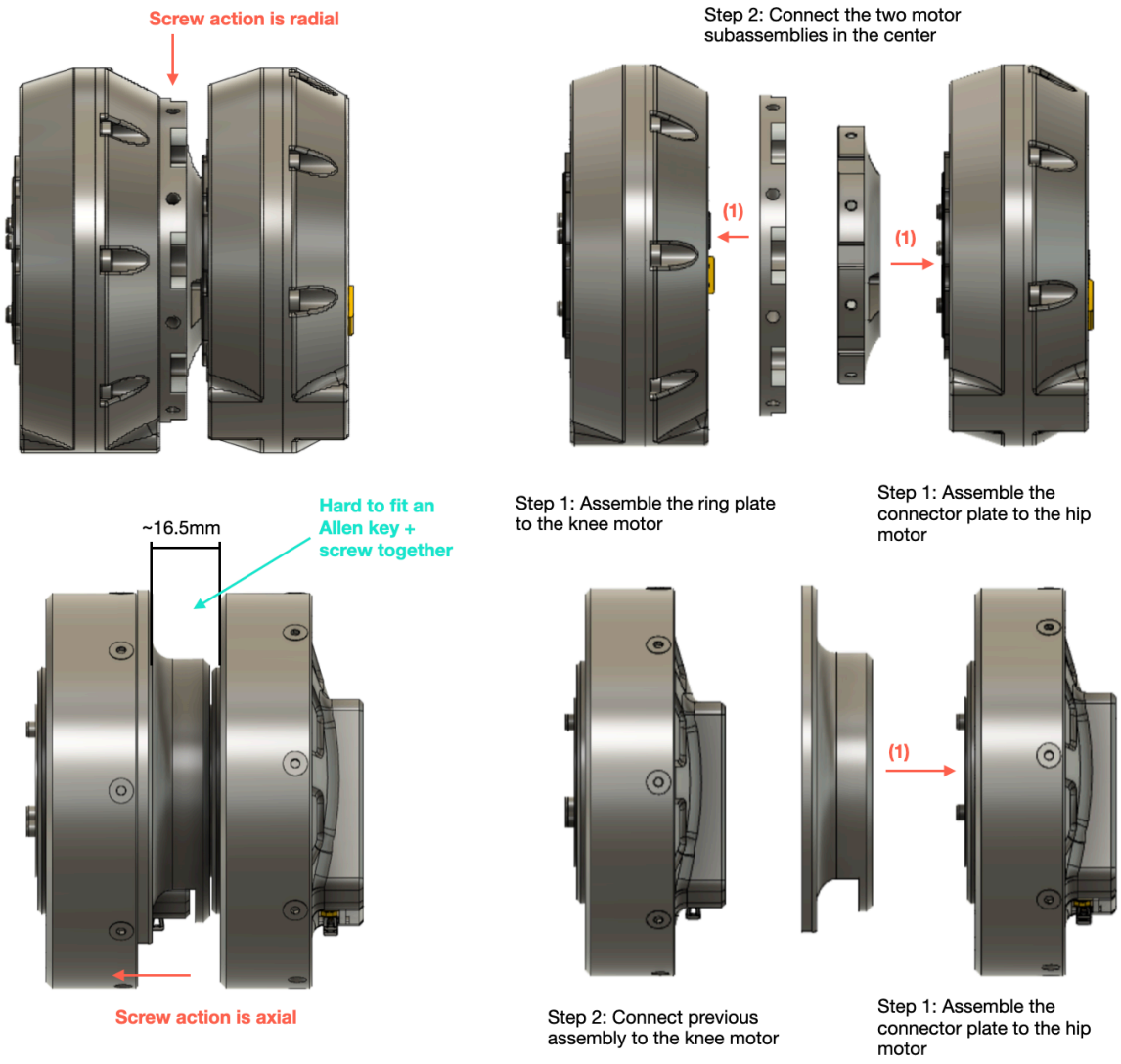

A.2.0 Effect of belt geometry + material properties on the stiffness of the belt. Much of the information was crowdsourced from the Biomimetics Lab knowledge base.

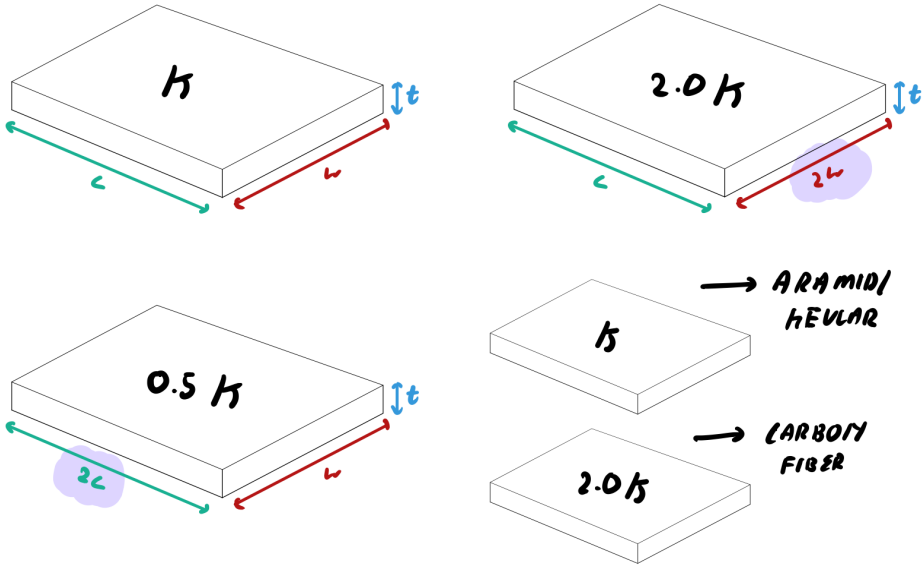

A.2.1 Motor belt resonant frequency diagram. The resonance results between the belt and the rotor of the motor assuming a locked knee joint. This frequency can be directly measured by hitting the leg against a stable and measuring rotor motions using the encoder on the motor module. In this case we assume the lower leg is fixed to the floor.

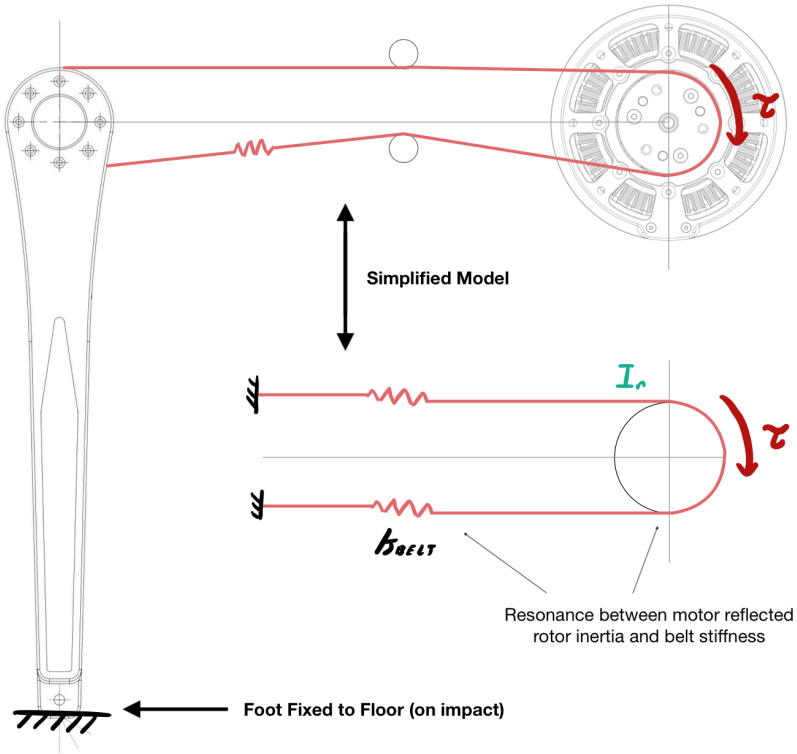

Appendix B.

B.1.0 U10 Torque Speed Curves including power map (left) and efficiency map (right). Note that these torque speed curves were measured on the dynamometer platform described in Section III using the procedure described in [10]. Note that these torque speed curves include the 6:1 gearbox. Note these curves were first published in [4].

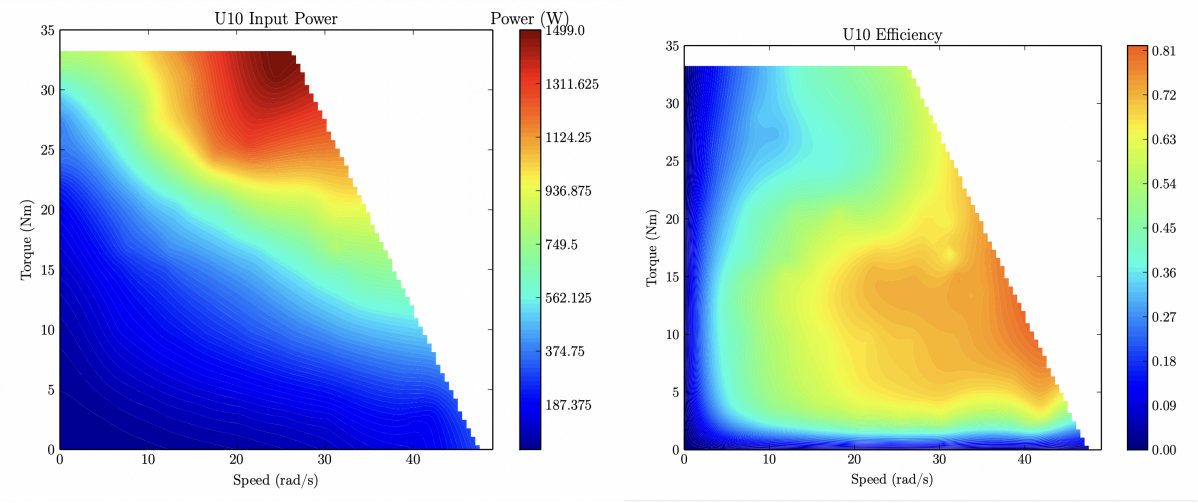

B.1.1 U8 Torque Speed Curves including power map (left) and efficiency map (right). Note that these torque speed curves were measured on the dynamometer described in [8] using the procedure described in [8]. Note that these torque speed curves DO NOT include the 6:1 gearbox. These curves were published in [8].

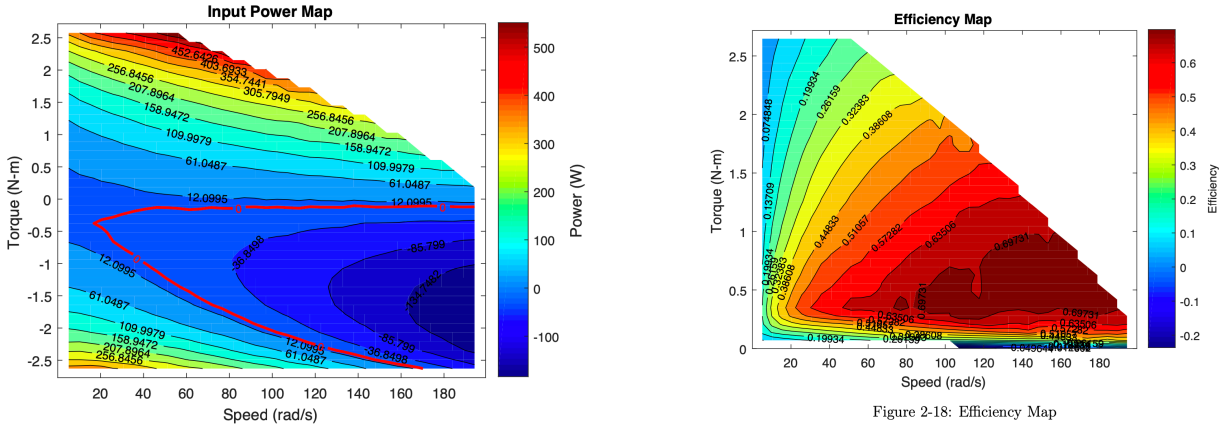

Figure 2-18: Efficiency Map

Acknowledgments.

Before we leave, there's a couple people I need to thank—in long form.

To Professor Sangbae Kim, thank you for taking me as a UROP in your lab, thank you for the resources, the mentor-ship, and for enabling me to complete this project. I've learned so much and I look forward to learning so much more in your lab in grad school.

To Elijah Stranger-Jones, thank you for being my supervisor, mentor, and friend every single day. Thank you for your belief and patience, for steering me in the right directions, and for giving me the space to fail and learn from my mistakes.

To Andrew, Steve, Matt, Charles, Liam, Meng, David, and the rest of the MIT Biomimetic Robotics Lab, thank you for the support, the friendship, and for all you've taught me.

To Jenny Zhang and Sanjna Ravichandar, thank you for being my table-mates in lab and keeping me company during all those late nights.

To Alex Hattori, thank you for helping me get started down this path in the lab and in the field of dynamic robots, I miss seeing you around the Edgerton Shop.

To Jack, Ashisha, Lisa, Francis, Maria, and the rest of my family on MIT Solar Car, at the MIT Edgerton Center, and MIT D-Lab (I can't list all of you, but I do mean all of you), thanks for everything.

To all my friends and family I made here at MIT and back at home, I love you and thank you for the support.

To Aashini Shah, thanks for all the advice on life and research. To Fiona Gillespie, thanks for being an amazing project partner and an even more amazing friend, I have learned so much from you.

To Fischer J Moseley, best friend I could've asked for, you rock, seriously.

To Sydney and Cameron, you're both amazing.

To Annemarie Dapoz, and Christopher Kiel, thanks for being here from the beginning.

And finally to Diane Li, Caroline Jordan, and Quang Kieu. I love you three so much, thank you for teaching me everything I know and for being there no matter what.